ACS OMEGA

http://pubs.acs.org/journal/acsodf

Article

Synthesis, Thermal Analysis, Spectroscopic Properties, and Degradation Process of Tutton Salts Doped with $AgNO_3$ or H_3BO_3

Tiago S. Pacheco,* Zélia M. C. Ludwig, Victor H. Oliveira, Ingrid D. Barcelos, Rafael L. de Souza, Edinei C. Paiva, Maximiliano D. Martins, Flavia C. Marques, Gustavo F. S. Andrade, and Santunu Ghosh*

Cite This: *ACS Omega* 2023, 8, 17800−17808

Read Online

ACCESS | Metrics & More | Article Recommendations | Supporting Information

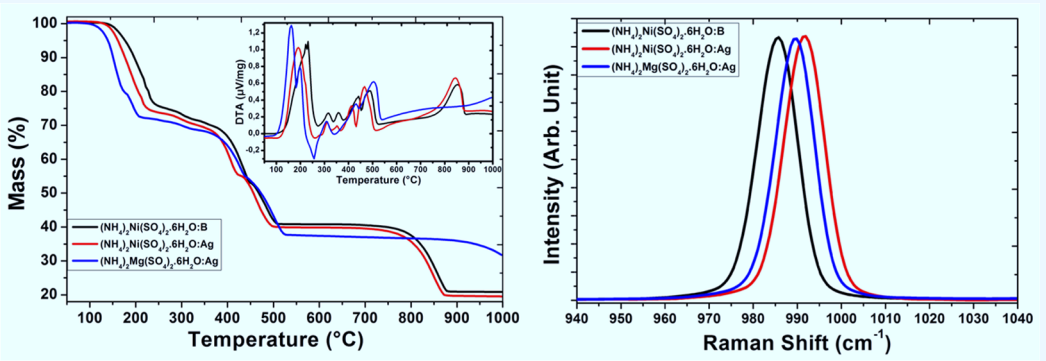

ABSTRACT: In this work, we synthesized and studied the spectroscopic properties of $(NH_4)_2(SO_4)_2Y(H_2O)_6$ (Y = Ni, Mg) crystals doped with $AgNO_3$ or H_3BO_3. These crystals constitute a series of hexahydrated salts known as Tutton salts. We investigated the influence of dopants on the vibrational modes of the tetrahedral ligands NH_4 and SO_4, octahedral complexes $Mg(H_2O)_6$ and $Ni(H_2O)_6$, and H_2O molecules present in these crystals through Raman and infrared spectroscopies. We were able to identify bands that are attributed to the presence of Ag and B dopants, as well as band shifts caused by the presence of these dopants in the crystal lattice. A detailed study of the crystal degradation processes was performed by thermogravimetric measurements, where there was an increase in the initial temperature of crystal degradation due to the presence of dopants in the crystal lattice. Raman spectroscopy of the crystal residues after the thermogravimetric measurements helped us to elucidate the degradation processes occurring after the crystal pyrolysis process.

1. INTRODUCTION

A wide variety of complex inorganic materials composed of bimetallic sulfates are well known in the scientific community, for example, dehydrated $A_2B_2(SO_4)_3$ complexes are known as the langbeinite phase, dihydrated complexes constitute the $A_2B(SO_4)_2{\cdot}2H_2O$ krohnkite phase, and tetrahydrate complexes are leonites $A_2B(SO_4)_2{\cdot}4H_2O$. In particular, hexahydrate complexes $A_2B(SO_4)_2{\cdot}6H_2O$ constitute the Tutton salt family, where A is a monovalent alkali metal or ammonium and B is a bivalent transition metal; S can be replaced by Se and H_2O by D_2O, as reported by Saha et al.[1]

Tutton salt crystals started to be studied by Alfred E. H. Tutton around 1890.[2−4] This family of isostructural crystals can assume a broad range of compositions with different properties. Interestingly, regardless of their chemical composition, this family of salts crystallizes in the monoclinic system with the spatial group $P2_1/c$ with two molecules occupying the unit cell $Z = 2$. The empirical formula that represents these crystals is $A_2B(YO_4)_2(H_2O)_6$, where A = Cs^+, K^+, NH_4^+, Rb^+, and Tl^+; B = Co^{2+}, Cu^{2+}, Fe^{2+}, Mn^{2+}, Ni^{2+}, V^{2+}, and Zn^{2+}; and Y = S, Se, and Cr, and can still be deuterated. These crystals can be used as optical filters to suppress transmission bands in the visible and allow passage in the UV region for wavelengths below 400 nm and IR for wavelengths between 700 and 1100 nm, mainly for transition metals Co, Cu, Fe, Mn, and Ni. Also, they can be used as radiation filters in UV/IR detectors used for military purposes in missile approach warning systems.[3,5,6]

The structure of Tutton salt is composed of SO_4^{2-} tetrahedrons and $M(H_2O)_6^{2+}$ octahedrons through hydrogen bonds of H_2O molecules and interconnected by monovalent cations K^+, Rb^+, Cs^+, or NH_4^+. These above types of

Received: January 30, 2023
Accepted: April 27, 2023
Published: May 8, 2023

Table 1. Masses in Grams of Precursor Reagents Used to Crystallize the Samples[a]

reagents	$(NH_4)_2SO_4$	$Mg(SO_4)\cdot 7H_2O$	$Ni(SO_4)\cdot 6H_2O$	$AgNO_3$	H_3BO_3
AMgSH:Ag	5.0003	9.3260		0.2004	
ANiSH:Ag	5.0030		9.9431	0.2014	
ANiSH:B	4.9988		9.9430		0.6142
molar mass (g mol^{-1})	132.14	246.47	262.85	169.87	61.83

[a]Molar masses are also given in the last line.

connections can be affected by agents such as dopants/impurities in the crystalline network of these materials. The presence of dopants can lead to changes in the normal vibrational modes of the molecular groups SO_4, NH_4, H_2O, and $M(H_2O)_6$.[7−9] In recent years, several studies have been reporting on the attempt of doping Tutton salt family crystals, in addition to theoretical−computational studies (density functional theory (DFT)) where band structures and calculations of vibrational frequencies were studied.[10−12] Notably, our team synthesized $K_2M(SO_4)_2(H_2O)_6$ mixed crystals, with M being a mixed composition of Ni/Co, to study the effects of a lithium dopant on the vibrational modes of the tetrahedral molecular groups SO_4 and octahedral $Ni(H_2O)_6$ and $Co(H_2O)_6$, as reported by Pacheco et al.[13]

Other studies provide insights into doped crystals of the Tutton salt family with rare-earth ions, and the properties of the emission/luminescent absorption processes of rare-earth ions were investigated and possible applications in nonlinear optics were evaluated.[7,14−17] Additionally, Abu El-Fadl et al.[18] introduced doping with small fractions of iodide ions and verified subtle changes in powder X-ray diffraction patterns, transmittance properties, thermal behavior of their samples, and unexpected second harmonic generation behaviors. In that sense, researchers who developed studies on Tutton salts are increasingly seeking to combine the properties of bivalent ions such as Co^{2+}, Ni^{2+}, Mg^{2+}, Mn^{2+}, and Cu^{2+} in the crystalline structure of mixed or even doped salts in order to improve some of its properties or even discover new properties.

Neto et al.[19] concluded in a new and interesting study that these crystals can be applied in thermochemical systems for thermal energy storage and also evaluated the empty spaces present in the unit cells of their crystals through electronic density isosurfaces, showing that high percentage of empty spaces can cause a decrease in the energy of interactions affecting physicochemical parameters such as solubility, dissolution, and hardness of crystalline structures. On the other hand, these empty spaces can be filled by dopants in order to strengthen these intermolecular interactions in order to increase, for example, the thermal stability of the crystals.

In the present study, we developed the synthesis of doped Tutton crystals using the crystal growth technique by slow isothermal evaporation. Moreover, we performed a study of the thermal and vibrational properties of silver-doped magnesium ammonium sulfate hexahydrate crystals (AMgSH:Ag), silver-doped nickel ammonium sulfate hexahydrate (ANiSH:Ag), and boron-doped nickel ammonium sulfate hexahydrate (ANiSH:B). Regarding the vibrational modes, our results were presented, discussed, and compared with the literature for pure crystals with similar compositions. In Raman spectra, we identified the vibrational modes of molecular groups SO_4, $M(H_2O)_6$, and H_2O. In addition, we were able to identify some bands that can be attributed to moieties containing Ag or B dopants, as well as band shifts caused by the presence of dopants in the crystal lattice. In thermogravimetric measurements, we verified that the crystals had significant gains in their initial dehydration temperatures caused by the presence of dopants. Furthermore, with Raman spectroscopy, the vibrational modes of the molecular groups that compose the structures of the oxide residues resulting from the thermogravimetric measurements were identified.

2. MATERIALS AND METHODS

Our samples of crystals $(NH_4)_2Mg(SO_4)_2\cdot 6H_2O$:$AgNO_3$ (AMgSH:Ag), $(NH_4)_2Ni(SO_4)_2\cdot 6H_2O$:$AgNO_3$ (ANiSH:Ag), and $(NH_4)_2Ni(SO_4)_2\cdot 6H_2O$:$H_3BO_3$ (ANiSH:B) were grown by the method of slow evaporation of the solvent in an aqueous solution with the temperature maintained at 40 °C. The precursor reagents for preparing the growth solutions were ammonium sulfate $(NH_4)_2SO_4$, 99% purity; nickel sulfate hexahydrate $Ni(SO_4)_2\cdot 6H_2O$, purity 98%; magnesium sulfate heptahydrate $Mg(SO_4)_2\cdot 7H_2O$, 99% purity; silver nitrate $AgNO_3$, 99.5% purity; and boric acid H_3BO_3, 99.5% purity.

The stoichiometric quantities of the starting materials are described in Table 1. After the reagent masses were measured, the solutions were prepared by dissolving the solids in 200 mL of deionized water with pH = 6 and R = 18.2 MΩ cm. To solubilize the reagents, the solution was heated up to a temperature of 50 °C and stirred for 1 h. Then, the solution was filtered on a filter paper (14 μm pores, 205 μm thickness, 80 g m^{-2}) and taken to an oven with a temperature of 40 ± 1 °C, where the growth process took place in an average time of 20 days.

The thermogravimetry/differential thermal analysis (TG/DTA) thermogravimetric analysis was performed using a NETZSCH model STA 449 F3 Jupiter calorimeter. The samples were ground using a ceramic mortar, and the measurements were carried out at a heating rate of 10 °C min^{-1}, covering the temperature range from 50 to 1000 °C, in an inert atmosphere of N_2 and a flow of 20 mL min^{-1}.

Raman spectra were acquired using a Bruker spectrometer, model SENTERRA, coupled to an Olympus microscope, with the excitation radiation at 632.8 nm from a HeNe laser and a laser power of 20 mW. For the acquisition of the Raman spectra, the sample at room temperature was placed on a rigorously cleaned glass slide. Data collection was performed using a 50× magnification objective lens (NA 0.51) and the acquisition time was 20 s.

Micro-FTIR measurements were performed using a Cary 620 FTIR spectromicroscopy from Agilent Technologies using a Globar source. Single-point reflectance spectra were collected in the mid-infrared range of 400−6000 cm^{-1}, with a spectral resolution of 8 cm^{-1}, signal reading by an MCT-100 μm detector, and a 25× objective lens with an approximately 400 × 400 μm^2 spot size. The final spectrum is an accumulation of 64 scans normalized by the spectrum of a clean Au surface as a background reference.

https://doi.org/10.1021/acsomega.3c00622
ACS Omega 2023, 8, 17800−17808

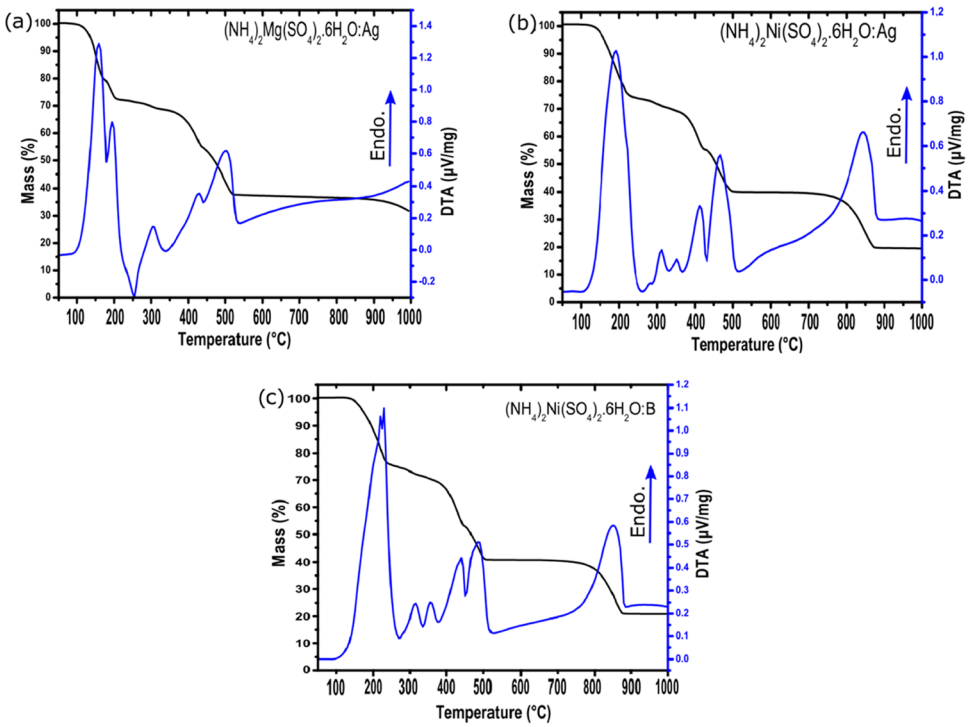

Figure 1. TG/DTA curves for the percentage of mass loss together with the endothermic peaks of temperature variation involved in each step of degradation of (a) AMgSH:Ag, (b) ANiSH:Ag, and (c) ANiSH:B crystals.

3. RESULTS AND DISCUSSION

Thermogravimetric analyses allowed a quantitative and qualitative study regarding all stages of the crystal degradation processes. In Figure 1, the TG/DTA curves of the obtained crystals are shown, where all stages of degradation of the crystals can be observed for each sample. The DTA curves in Figure 1a−c (samples AMgSH:Ag, ANiSH:Ag, and ANiSH:B) show two endothermic DTA peaks during dehydration in the temperature range of 100−270 °C. These crystals also acquire the anhydrous langbeinite crystalline phase $(NH_4)_2M(SO_4)_2$:X, where M = Mg and Ni and X = B and Ag. In the temperature range of 250−540 °C, four endothermic peaks appear in the DTA curves, referring to the decomposition of NH_4^+, H_3BO_3, or $AgNO_3$ and of a SO_4^{2-} moiety into SO and O_2. In the last degradation step, in the temperature range of 745−890 °C, one may observe that an endothermic peak appears in the DTA curves of the samples ANiSH:Ag and ANiSH:B (Figure 1b,c), referring to the decomposition of one mol equivalent of SO_4^{2-} into SO_2 and $(1/2)O_2$. However, for sample AMgSH:Ag (Figure 1a), the decomposition of the SO_4^{2-} molecule seems to start around 890 °C going up to 1000 °C, decomposing one-third of the SO_4^{2-} mol equivalent. Accompanying these figures, in Tables S1−S4, we present a detailed description of the theoretical values of the percentages of crystal mass losses in comparison with the values obtained experimentally for the chemical reactions that occur during each step of crystal degradation.

All degradation steps for each sample are described in detail in Tables S1−S4, where we presented the initial dehydration temperature and DTA peak position. The percentage values of ideal mass losses (%) were calculated from the empirical formula of each crystal, adding the atomic masses of the amounts of each chemical element present in that formula; then, the proportionality % is attributed to each element or molecule that the sample expels in gaseous form during its degradation process.

It can be seen from the DTA curve of Figure 1 that each mass loss is accompanied by endothermic peaks. Analyzing the degradation processes of samples AMgSH:Ag, ANiSH:Ag, and ANiSH:B, shown in Figure 1a−c, and the assignment of the mass in TG and peaks in DTA present in Tables S1−S4, one may observe that in the temperature range between 110 and 230 °C, the samples suffered a mass loss of approximately 17−26%, corresponding to the mass of six molecules of H_2O, present in the crystal structure. For the other samples AMgSH:Ag, ANiSH:Ag, and ANiSH:B, the second degradation step is equivalent to approximately 16−23% and occurs between 240 and 506 °C; the decomposition sequence corresponds to the loss of 2 mol equiv of NH_3, one H_2O, and one SO_2. The last degradation step occurs in the temperature range of 520−890 °C for ANiSH:Ag and ANiSH:B samples, resulting from the decomposition of the SO_4^{2-}, equivalent to 17−19% mass loss. Conversely, sample AMgSH:Ag suffers a partial degradation of one SO_4^{2-}, corresponding to approximately 6% mass loss. The final residues in samples AMgSH:Ag, ANiSH:Ag, and ANiSH:B after thermal treatment were $Mg(1/2)SO_2Ag(1/3)O_2$ and NiO_3, respectively. The residual substances were confirmed through Raman spectroscopy because the vibrational modes of the oxides present in these residues were identified (a detailed discussion may be found below).

Comparing the initial degradation temperature, we observed an increase in the samples ANiSH:B and ANiSH:Ag, with temperature gains of 39 and 36 °C, respectively, while the dehydration temperature of the pure crystal $(NH_4)_2Ni(SO_4)_2 \cdot 6H_2O$ was 96 °C, as reported by Pacheco et al.[7] For sample AMgSH:Ag, the temperature gain was 24 °C compared to the similar pure crystal, which is 70 °C, as reported by Souamti et al.[20]

https://doi.org/10.1021/acsomega.3c00622
ACS Omega 2023, 8, 17800−17808

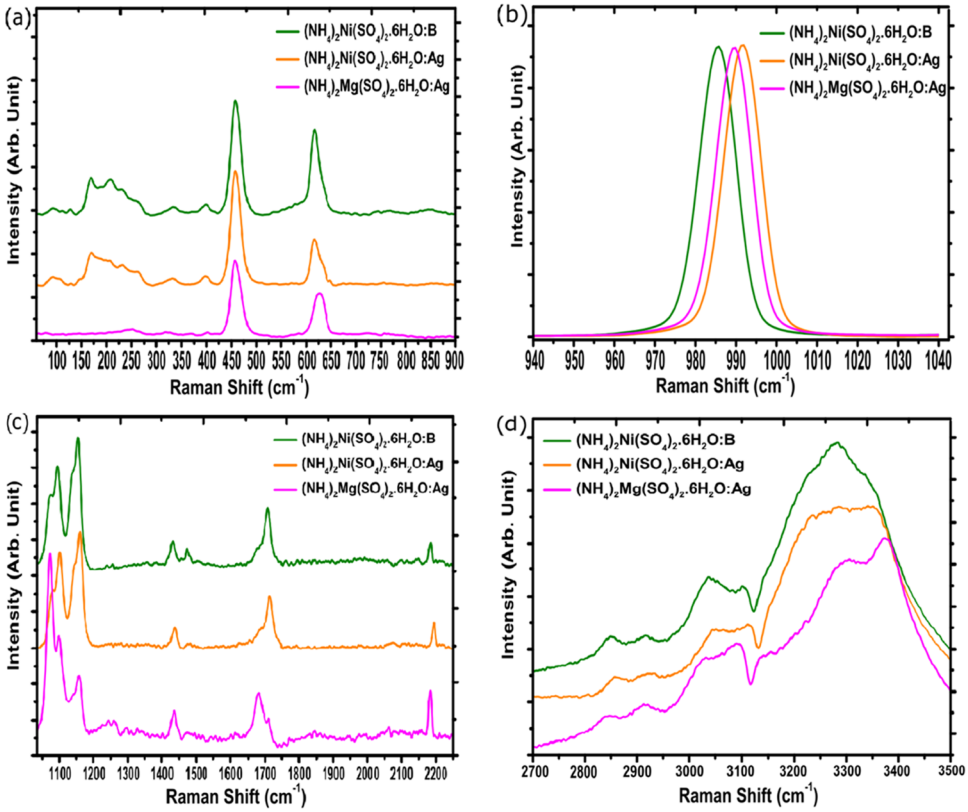

Figure 2. Raman spectra of samples ANiSH:B, ANiSH:Ag, and AMgSH:Ag (green, yellow and pink curves, respectively) in the ranges of (a) 70−900 cm^{-1}, (b) 925−1040 cm^{-1}, (c) 1040−2250 cm^{-1}, and (d) 2700−3500 cm^{-1}. We observed the bands related to the vibrational modes of molecular groups H_2O, NH_4^+, $(SO_4)_2^{2-}$, and $M(H_2O)_6^{2+}$.

Raman measurements in the range of 100−3500 cm^{-1} were performed in all samples, as shown in Figure 2, using an excitation laser of 632.8 nm. These crystals have 234 normal vibrational modes, considering the structure of SO_4, NH_4, H_2O, and $M(H_2O)_6$ groups, including three acoustic modes, being $1A_u + 2B_u$. According to the group theory, the irreducible representation for the optical phonons of these crystals is given by: $\Gamma = 57A_g + 57B_g + 60A_u + 60B_u$, where only A_g and B_g modes are active in Raman, adding a total of 114 modes, and A_u and B_u modes are active in IR, adding up to 120 modes.[8−10,21,22]

Specially doped crystals can present peculiar changes in the vibrational modes resulting from molecular interactions in the crystalline structure of these salts. In these crystalline structures, SO_4 tetrahedral is present, which is linked to the $M(H_2O)_6$ octahedral by means of O−H···O hydrogen bonds between the hydrogen atoms belonging to the water molecules and the oxygen atoms of SO_4; the NH_4 tetrahedral is coordinated with the SO_4 tetrahedral, forming the entire crystal lattice.[10,21,23]

Table 2 exhibits the position of Raman bands from Figure 2 and the assignment of the groups H_2O, NH_4^+, $(SO_4)_2^{2-}$, and $M(H_2O)_6^{2+}$ to the samples ANiSH:B, ANiSH:Ag, and AMgSH:Ag. The results agree with the values presented in previous studies by Barashkov et al.[8] and Ghosh et al.[10]

The Raman measurements of the doped crystals in Figure 2 reveal changes compared to similar systems in the same crystal family that do not have any doping. These differences can be attributed to distortions in the bond lengths of the octahedral $M(H_2O)_6^{2+}$ and tetrahedral NH_4^+ and $(SO_4)_2^{2-}$ caused by the influence of dopants introduced into the crystal lattice. According to Table 2, there was a marked difference for the ν_1 mode of $(SO_4)_2^{2-}$ in all samples, especially for samples ANiSH:B (with boron doping) and ANiSH:Ag (with silver doping) since these two are the samples with the closest composition to the nondoped crystal. One may notice that in the Raman spectrum of the crystal $(NH_4)_2Ni(SO_4)_2{\cdot}6H_2O$, there is a band at 981 cm^{-1} that may be assigned to the symmetrical mode of SO_4 Ghosh et al.,[10] while for ANiSH:B- and ANiSH:Ag-doped samples, this band appears centered at 985 and 991 cm^{-1}, respectively. This band shift is caused by the presence of dopants that possibly change the local electron density in the vicinity of SO_4, causing a higher vibrational frequency, that is, shifting the band to higher wavenumbers. In addition, the vibrational mode characteristics of the $AgNO_3$ and H_3BO_3 dopants present in the crystalline structures of the crystals were also identified.

Complementary to the Raman spectroscopy results, spectroscopic measurements were performed in the mid- and near-infrared region, as shown in Figure 3. The analysis of spectra in the mid-infrared region is quite common for Tutton salts. However, for the near-infrared (NIR) region, no studies were found in the literature presenting results for this infrared range. The NIR spectra of the analyzed samples show two broad spectral bands, which arise from the presence of water, which present different coordination with the molecules in their vicinity.

The wide bands appearing in this region of the infrared spectrum are assigned to M−OH vibrational modes and also to combinations of H−O and N−H modes, as described at the end of Table 3, according to the refs 29 and 30. The bands centered at 2340 and 2361 cm^{-1}, visualized in the spectra

https://doi.org/10.1021/acsomega.3c00622
ACS Omega 2023, 8, 17800−17808

Table 2. Band Wavenumber (cm^{-1}) and Vibrational Assignment for the Raman Spectra of ANiSH:B, ANiSH:Ag, and AMgSH:Ag[a]

band wavenumber (cm^{-1})			literature		
ANiSH:B	ANiSH:Ag	AMgSH:Ag	8	10	assignment
112; 127	106; 127	112	110; 121	105; 113	$SO_4^{(L)}$
	145	145	131	122; 138	
168	169		161	163	$NH_4^{(L)}$
188	188		170; 183	183	$*(\nu_5)$
207	207		196; 203	205	$NH_4^{(L)}$
230	231		218; 235		$*(\nu_5)$
261	262	251	253	241	$*(\nu_2)$
334	333	323	300; 313		$H_2O^{(Tw)}$
371	364	369			$NH_4^{(L)}$
399	398	402	384	393	$*(\nu_1)^{(ss)}$
458	458	457	451, 457	455	$(\nu_2)\ SO_4^{(sb)}$
578	574	585	577	579	$H_2O^{(w)}$
617; 635	616; 633	623; 631	616; 627	610; 624	$(\nu_4)\ SO_4^{(ab)}$
	755	756			$^{(sb)}(\nu_4)\ AgNO_3$[24,25]
743; 769	769		743; 807	839	$H_2O^{(r)}$
847; 880					$^{(ss)}H_3BO_3$[26−28]
	857; 890				$AgNO_3$[24,25]
985	991	989	983	981	$(\nu_1)\ SO_4^{(ss)}$
1023	1021	1022			$(\nu_1)\ AgNO_3$[24,2526−28]
1035	1038	1042			H_3BO_3[26−28]
1073	1080	1172	1072	1068	$(\nu_2 + \nu_4)\ SO_4$
1094	1100	1098	1093	1090	$(\nu_3)\ SO_4^{(as)}$
1137	1144	1139	1136	1136	
1154	1159	1158	1152	1150	
1430	1436	1433	1432	1426	$(\nu_4)\ NH_4^{(ab)}$
1472	1480		1467		
1675	1684	1680	1676	1670	$(\nu_2)\ (NH_4{-}H_2O)^{(sb)}$
1707	1714	1712	1709	1707	$NH_4\ (\nu_2)^{(sb)}$
2180	2194	2183			$(\nu_2 + L)\ NH_4$[22]
2850	2860	2845	2842	2845	$(2\nu_4)\ NH_4$
2916	2923	2915	2918		$(\nu_1)\ NH_4$
3038	3049	3026	3035	3035	$(\nu_3)\ NH_4$
3102	3112	3091	3100	3109	$(\nu_1)\ H_2O$
3141	3176	3150	3138		$(\nu_3)\ H_2O$
3224	3232	3222	3232	3273	
3280	3287	3300			$(\nu_1)\ H_2O$
3336	3344	3370	3364		$(\nu_3)\ H_2O$

[a]T = translation, L = libration, * = octahedral complex $M(H_2O)_6^{2+}$, tw = twisting, r = rocking, w = wagging, ss = symmetric stretching, sb = symmetric bending, ab = asymmetric bending, and as = asymmetric stretching.

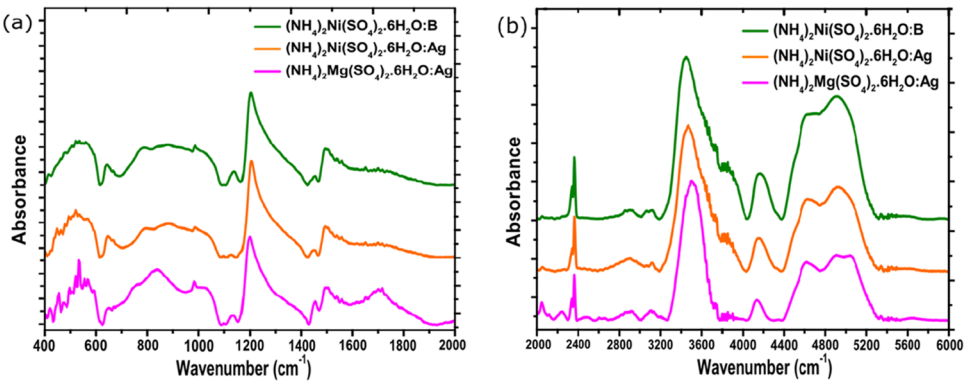

Figure 3. Absorption spectra for samples ANiSH:B, ANiSH:Ag, and AMgSH:Ag obtained at (a) 400−2000 cm^{-1} in the mid-infrared region (400−4000 cm^{-1}) and (b) 2000−6000 cm^{-1} in the initial near-infrared range (4000−6000 cm^{-1}).

https://doi.org/10.1021/acsomega.3c00622
ACS Omega 2023, 8, 17800−17808

Table 3. Band Assignment for Near-Infrared Spectra of ANiSH:B, ANiSH:Ag, and AMgSH:Ag[a]

band wavenumber (cm^{-1})			literature		
ANiSH:B	ANiSH:Ag	AMgSH:Ag	8	10	assignment
440; 447	440; 447	440; 455	438; 457	438; 450	(ν_2) $SO_4^{(sb)}$
534; 568	534; 568	533; 568	544	549; 569	$H_2O^{(L)}$
642	646	651	615	614	(ν_4) $SO_4^{(ab)}$
667	667	670	627; 690	625	
728	761; 794	741; 759	725	744	$H_2O^{(r)}$
786	848	790; 815	743	769	
848; 882	882	837; 882	807	770	
987	987	983	983	980	(ν_1) $SO_4^{(ss)}$
1036	1036	1036		1034	($\nu_2 + \nu_4$) SO_4
1099	1096	1099	1085	1094	(ν_3) $SO_4^{(as)}$
1139	1127	1134	1144	1145	
1203	1205	1199		1274	
1453	1450	1454	1445	1432	(ν_4) $NH_4^{(ab)}$
1494	1494	1494	1465	1468	
1703	1703	1703	1709	1709	H_2O-NH_4 (ν_2)$^{(sb)}$
2449	2051	2047			(ν_2 + L) NH_4
		2117	2115		($\nu_2 + \nu_3$) SO_4
		2240	2240		($2\nu_3$) SO_4
2340	2340	2340			CO_2 da atmosfera ambiente
2361	2361	2361			
2900	2900	2900			($2\nu_4$) NH_4
3108	3108	3108			(ν_3) $NH_4^{(as)}$
			3364		(ν_1) $H_2O^{(ss)}$
3445	3465				(ν_3) $H_2O^{(as)}$
		3506			(ν_1 + L) H_2O
4166	4136	4150	4000 a 4400		Y−OH[29,30]
4227	4185	4226			
4336	4342	4331			
4499	4499	4499	4500 a 7000		H−O e N−H combinação de modos (sb + ss)[29,30]
4616	4611	4611			
4916	4921	4906			
5034	5085	5040			
5341	5341	5341			
5631	5631	5646			

[a]T = translation, L = libration, * = octahedral complex $M(H_2O)_6^{2+}$, tw = twisting, r = rocking, w = wagging, ss = symmetric stretching, sb = symmetric bending, ab = asymmetric bending, and as = asymmetric stretching.

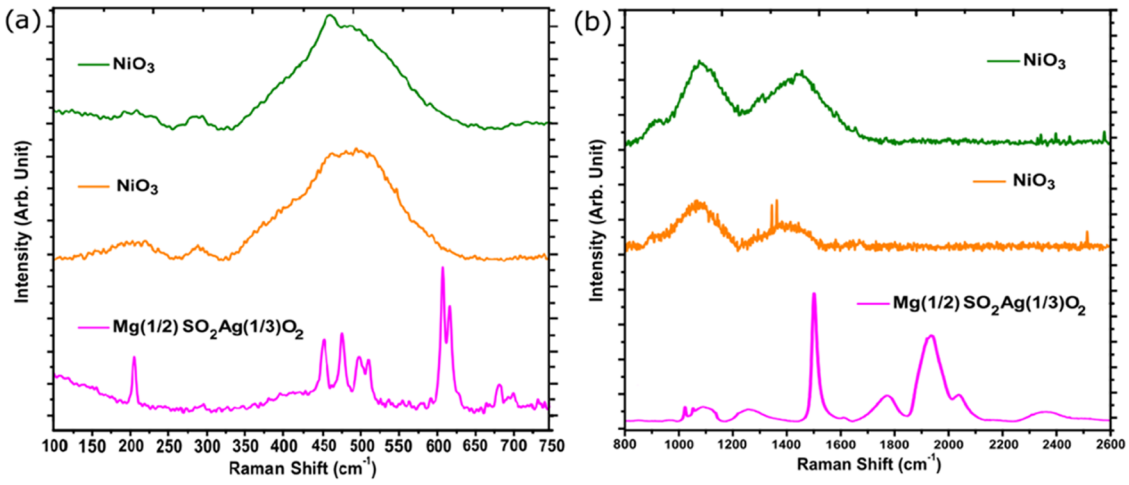

Figure 4. Raman spectra of sample oxide residues left over after thermogravimetric measurements: (a) 100−750 cm^{-1} and (b) 800−2600 cm^{-1}.

shown in Figure 3, are characteristic of the asymmetric axial deformation of the O═C═O of the ambient atmosphere where the measurements were taken. The characteristic bands of deformations of the NH bond appear close to 2900 cm^{-1}. For all samples, the frequencies of the two fundamental OH stretching vibrations, ν_1 and ν_3, and the bending vibration, $2\nu_2$,

https://doi.org/10.1021/acsomega.3c00622
ACS Omega 2023, 8, 17800−17808

of the H_2O molecule are very close and cause an intermolecular coupling that occurs between similar vibrations of neighboring molecules; for these hydrated salts, this proximity causes strong broadening and general distortion of all forms of bands above 3200 cm^{-1}. The same effect occurs in the region above 4000 cm^{-1} for fundamental vibrations associated with hydrogen−oxygen vibrations associated with water in the case of minerals and hydrated inorganic compounds such as Tutton salts.[29,30]

Supporting the information obtained previously through the thermogravimetric measurements, Raman measurements of the residues from the thermogravimetric measurements were obtained. This study confirms the composition of the oxide residues of the crystals after all degradation processes by identifying their characteristic vibrational modes. The Raman spectra for the thermal treatment residues are shown in Figure 4a, showing bands corresponding to the oxides Ni−O, O_2−Ni−O_2, and O−NiO−O.[31−34] For the residues of the ANiSH:B and ANiSH:Ag samples, the band at 695 cm^{-1} is assigned to Ni−O−Ni bonds;[33] the bands at 520 and 584 cm^{-1} are attributed to torsion and stretching of the Ni−O bonds, respectively. In addition, there is a broad band in the 900−1200 cm^{-1} range, which is attributed to $Ni(O_2)_2$; there are also two bands, one at 1096 cm^{-1} and another weak band at 1460 cm^{-1}, both assignable to O−Ni−O−O.[31]

It is clearly noted that ANiSH:B and ANiSH:Ag samples have NiO_3 residues, as their compositions are very similar, and it was not possible to make a distinction in their spectra based on the effects of their dopants B and Ag. On the other hand, as expected, the $Mg_{1/2}SO_2Ag_{1/3}O_2$ residue has distinct Raman spectra, as it did not undergo complete degradation until reaching a temperature of 1000 °C, leaving SO_2 molecules in its structure that did not wholly decompose during thermogravimetric measurements.

Residues containing boron and silver from ANiSH:B and ANiSH:Ag, respectively, present broad bands at 206, 458, and 486 cm^{-1}, which may be associated with the translation of NiO in both. The bond at 724 cm^{-1} on the ANiSH:B residue, at 738 cm^{-1} on the ANiSH:Ag residue, and two bands at 905 and 1075 cm^{-1} on both residues were observed. In the region between 1250 and 1500 cm^{-1}, we have two bands, one at 1310 cm^{-1} and one at 1450 cm^{-1}, which corresponds to O−Ni−O−O.[31]

The Raman spectrum of the $Mg_{1/2}SO_2Ag_{1/3}O_2$ residue in Figure 4 has characteristic bands of the groups Mg−O, SO, Ag−O, and Ag−S, as described in Table 4. The bands assigned to SO and Mg−O bonds in the $Mg_{1/2}SO_2Ag_{1/3}O_2$ residue appear slightly shifted compared to the bands we had for the crystal before it underwent degradation in thermogravimetry. The bands between 650 and 900 cm^{-1} and 1900 and 2400 cm^{-1} are characteristic of water absorption from the ambient atmosphere since the residue has hygroscopic properties. In the region that goes from 1060 to 1400 cm^{-1}, we have broad bands associated with SO, Mg−O, and Ag−O bonds, which are difficult to associate with any vibrational mode of the residue due to the widening caused by the absorption of water, resulting in a change in the structural environment.

The results are consistent with the oxide residues proposed left over after all of the degradation steps of the samples in Tables S2−S4, in which all of the characteristic vibrational modes of these oxide residues were identified.

Table 4. Vibrational Modes Observed Via Raman Spectroscopy of the $Mg_{1/2}SO_2Ag_{1/3}O_2$ Residue[a]

Raman bands (cm^{-1})	assignment to groups
205, 295	$Ag-S^{(ss)}$ [35]
400	Mg−O
451	$O-S-O^{(sb)}$
474	Ag−O
497	Ag−S[35]
510	Mg−O
607, 615	$O-S-O^{(ab)}$
681, 699, 797	H_2O (absorbed from the environment)
850	Ag−OH
964	$S-O^{(ss)}$
1023, 1052	S−O
1060 a 1150	$S-O^{(as)}$, Mg−O, Ag−O
1180 a 1400	Mg−O e Ag−O
1501, 1612	Ag−O[35]
1772	S−O
1934, 2037, 2355	H_2O (absorbed from the environment)

[a]ss = symmetric stretching, sb = symmetric bending, ab = asymmetric bending, and as = asymmetric stretching.

4. CONCLUSIONS

In this manuscript, we described the synthesis and characterization of Tutton crystals doped with H_3BO_3 and $AgNO_3$, resulting in crystals of $(NH_4)_2Ni(SO_4)_2{\cdot}6H_2O$:B, $(NH_4)_2Ni(SO_4)_2{\cdot}6H_2O$:Ag, and $(NH_4)_2Mg(SO_4)_2{\cdot}6H_2O$:Ag. Thermogravimetric measurements allowed us to determine in detail the crystal degradation process up to 1000 °C, which allowed us to infer the chemical reactions that occur in each step of these processes, which are rarely reported in the literature on Tutton salts.

In addition, for these crystals, there were significant gains in dehydration temperature, which were 39, 36, and 24 °C in the crystals $(NH_4)_2Ni(SO_4)_2{\cdot}6H_2O$:B, $(NH_4)_2Ni(SO_4)_2{\cdot}6H_2O$:Ag, and $(NH_4)_2Mg(SO_4)_2{\cdot}6H_2O$:Ag, respectively, when compared with their equivalent crystals, without the influence of dopants on their structure. These considerable increases in the initial dehydration temperatures of the crystals are due to the effect of dopants on their crystal lattice, which makes them more thermally stable than conventional crystals without doping. In this sense, the Tutton salts with the doping investigated in this work may be promising materials for applications as windows for UV−IR radiation, as they are more thermally stable when compared to pure crystals of the Tutton salt family.

Concerning the Raman and infrared spectroscopic measurements, we identified the vibrational modes of H_2O, NH_4^+, SO_4^{2-}, and $M(H_2O)_6^{2+}$ groups from the crystalline structures of the synthesized crystals. Furthermore, we noted significant shifts in some bands related to these groups. The observed shifts were associated with the presence of dopants in the crystal lattice that cause distortions in the electronic densities of these molecular groups. Also, it was possible to identify characteristic bands related to the dopants. Moreover, complementary to the thermogravimetric measurements, Raman measurements of the residues confirmed that residues $(NH_4)_2Ni(SO_4)_2{\cdot}6H_2O$:B and $(NH_4)_2Ni(SO_4)_2{\cdot}6H_2O$:Ag were basically composed of NiO_3 oxides. For residue $(NH_4)_2Mg(SO_4)_2{\cdot}6H_2O$:Ag, on the other hand, it was evident that samples did not completely decompose in the temperature range from 50 to 1000 °C. From the Raman results, it was

https://doi.org/10.1021/acsomega.3c00622
ACS Omega 2023, 8, 17800−17808

possible to verify that the decomposition product was $Mg_{1/2}SO_2Ag_{1/3}O_2$.

The Raman results assigned the normal modes of vibration corresponding to chemical bonds Ni−O, Mg−O, Ag−O, Ag−S, and S−O, confirming the presence of dopants in the chemical composition of each residue of each crystal. It should be mentioned that some bands did not appear in the Raman spectra of the crystals before undergoing thermal degradation but appeared in the spectra of the residues. The study of residues of Tutton salts through spectroscopic techniques is still poorly explored in the literature. Therefore, our investigation opens the avenue to complement the understanding of the degradation processes of these materials.

■ ASSOCIATED CONTENT

Supporting Information

The Supporting Information is available free of charge at https://pubs.acs.org/doi/10.1021/acsomega.3c00622.

Initial dehydration temperatures and other degradation steps and description of the chemical reactions of each step of the sample degradation process: AMgSH:Ag, ANish:Ag, and AMgSH:B (PDF)

■ AUTHOR INFORMATION

Corresponding Authors

Tiago S. Pacheco − *Department of Physics, Federal University of Juiz de Fora, Juiz de Fora 36036-330 MG, Brazil; Centro Federal de Educação Tecnológica de Minas Gerais—Unidade Curvelo, Curvelo 35790-636 MG, Brasil;* orcid.org/0000-0002-0798-8184; Email: tspacheco@ymail.com

Santunu Ghosh − *Brazilian Center for Physical Research, CBPF, Rio de Janeiro 22290-180 RJ, Brazil;* orcid.org/0000-0002-2666-9461; Email: santunug@gmail.com

Authors

Zélia M. C. Ludwig − *Department of Physics, Federal University of Juiz de Fora, Juiz de Fora 36036-330 MG, Brazil*

Victor H. Oliveira − *Department of Physics, Federal University of Juiz de Fora, Juiz de Fora 36036-330 MG, Brazil*

Ingrid D. Barcelos − *Brazilian Synchrotron Light Laboratory (LNLS), Brazilian Center for Research in Energy and Materials (CNPEM), Campinas 13083-970 SP, Brazil;* orcid.org/0000-0002-5778-7161

Rafael L. de Souza − *Centro de Desenvolvimento da Tecnologia Nuclear, Belo Horizonte 31270-901 MG, Brazil; Federal University of Vales do Jequitinhonha e Mucuri, Janaúba 39440-000 MG, Brazil*

Edinei C. Paiva − *Centro de Desenvolvimento da Tecnologia Nuclear, Belo Horizonte 31270-901 MG, Brazil; Instituto Federal do Norte de Minas Gerais-Campus Januária, Januária 39480-000 MG, Brazil*

Maximiliano D. Martins − *Centro de Desenvolvimento da Tecnologia Nuclear, Belo Horizonte 31270-901 MG, Brazil;* orcid.org/0000-0003-4010-8043

Flavia C. Marques − *Department of Chemistry, Federal University of Juiz de Fora, Juiz de Fora 36036-330 MG, Brazil*

Gustavo F. S. Andrade − *Department of Chemistry, Federal University of Juiz de Fora, Juiz de Fora 36036-330 MG, Brazil;* orcid.org/0000-0003-0718-9400

Complete contact information is available at: https://pubs.acs.org/10.1021/acsomega.3c00622

Notes

The authors declare no competing financial interest.

■ ACKNOWLEDGMENTS

The authors acknowledge the financial support from the Brazilian agencies Fundação de Amparo à Pesquisa do estado de Minas Gerais (FAPEMIG), Conselho Nacional de Desenvolvimento Cientifico e Tecnológico (CNPq), and Financiadora de Estudos e Projetos (FINEP) contrato CT-Infra 01.14.0015.00, referência 0633/13. The authors also would like to acknowledge the IMBUIA beamline at Brazilian Synchrotron Light Laboratory (LNLS) for providing the micro-FTIR facility. T.S.P., V.H.O., and F.C.M. thank the Coordenação de Aperfeiçoamento de Pessoal de Nível Superior (CAPES) for their doctoral scholarships. Santunu Ghosh acknowledges Prof. Alexandre Mello and PCI for the research scholarship and support.

■ REFERENCES

(1) Saha, D.; Madras, G.; Guru Row, T. N. Manipulation of the hydration levels in minerals of sodium cadmium bisulfate toward the design of functional materials. *Cryst. Growth Des.* **2011**, *11*, 3213−3221.

(2) Alfred Edwin Howard Tutton, 1864 - 1938. *Obituary Not. Fellows R. Soc.* 1939, *2* (7), 621−626. DOI: 10.1098/rsbm.1939.0022.

(3) Pacheco, T. S.; Ghosh, S.; de Oliveira, M.; Barbosa, A. A.; Perpétuo, G. J.; Franco, C. J. Growth and characterization of potassium cobalt nickel sulfate hexahydrate crystals: A new UV light filter. *J. Sci.: Adv. Mater. Devices* **2017**, *2*, 354−359.

(4) Pacheco, T. d. S. Crescimento e caracterização de cristais de K com composição mista de Ni e Co da família do sal de Tutton. Dissertação (Mestrado em Ciências − Física de Materiais), Instituto de Ciências Exatas e Biológicas, Universidade Federal de Ouro Preto: Ouro Preto, 2015.

(5) He, Y.; Su, G.; Yu, X.; Li, Z.; Huang, B.; Jang, R.; Zhao, Q. Growth of α-nickel sulphate hexahydrate for ultraviolet filters. *J. Cryst. Growth* **1996**, *169*, 193−195.

(6) de Oliveira, M.; Ghosh, S.; Pacheco, T. S.; Perpétuo, G. J.; Franco, C. J. Growth and structural analysis of ammonium nickel cobalt sulfate hexahydrate crystals. *Mater. Res. Express* **2017**, *4*, No. 105036.

(7) Pacheco, T. S.; Ludwig, Z. M. C.; Ghosh, S.; Oliveira, V. H.; Sant'Anna, D. R.; Costa, C. B.; Lopes, R.; Oliveira, S. O.; Saint'Pierre, T. D.; Sousa, R. A.; Paiva, E. C. Growth, characterization and vibrational spectroscopy of (NH4)2NixMn(1−x)(SO4)2.6H2O:Nd crystals. *Mater. Res. Express* **2019**, *6*, No. 096302.

(8) Barashkov, M. V.; Komyak, A. I.; Shashkov, S. N. Vibrational spectra and crystal lattice dynamics of hexahydrates of zinc potassium and ammonium sulfates. *J. Appl. Spectrosc.* **2000**, *67*, 216−225.

(9) Barashkov, M. V.; Zazhogin, A.; Komyak, A.; Shashkov, S. Low-frequency vibrational spectra of crystals of tutton salts. *J. Appl. Spectrosc.* **2000**, *67*, 605−611.

(10) Ghosh, S.; Ullah, S.; de Mendonça, J. P.; Moura, L. G.; Menezes, M. G.; Flôres, L. S.; Pacheco, T. S.; de Oliveira, L. F.; Sato, F.; Ferreira, S. O. Electronic properties and vibrational spectra of (NH4) 2M ″(SO4) 2·6H2O (M ″= Ni, Cu) Tutton's salt: DFT and experimental study. *Spectrochim. Acta, Part A* **2019**, *218*, 281.

(11) Pacheco, T. S.; Ludwig, Z. M. C.; Ullah, S.; de Mendonça, J. P. A.; Sato, F.; de Souza, R. L.; Paiva, E. C.; Martins, M. D.; Marques, F. C.; Andrade, G. F. S.; Ghosh, S. Magnetic characterization, electronic structure and vibrational properties of (NH4)2 M(SO4)2·6H2O (M = Mn, Ni) crystals. *Solid State Commun.* **2021**, *334*−*335*, No. 114384.

(12) Narsimhulu, M.; Ramesh, G.; Haranath, D. A strong blue light-emitting material K2Ni (SO4) 2· 6H2O: Photoluminescence and magnetic properties. *Chem. Phys. Lett.* **2020**, *755*, No. 137792.
(13) Pacheco, T. S.; Ludwig, Z. M.; Sant'Anna, D. R.; Perpétuo, G. J.; Franco, C. J.; Paiva, E. C.; Ghosh, S. Growth and vibrational spectroscopy of K2LiyNixCo1-xSO42. 6H2O (y = 0.1; 0.2; 0.3; 0.4) crystals. *Vib. Spectrosc.* **2020**, *109*, No. 103093.
(14) Marzougui, H.; Martin, I.; Attia-Essaies, S.; Hassen-Chehimi, D. B.; Lalla, E.; Léon-Luis, S. Site selective luminescence of Eu3 + ions in K2Mg (SO4) 2·6H2O crystal. *Opt. Mater.* **2015**, *46*, 339−344.
(15) Souamti, A.; Martín, I.; Zayani, L.; Hernández-Rodríguez, M.; Soler-Carracedo, K.; Lozano-Gorrín, A.; Chehimi, D. B. H. Blue up-conversion emission of Yb3 +-doped langbeinite salts. *Opt. Mater.* **2016**, *53*, 190−194.
(16) Souamti, A.; Martín, I.; Zayani, L.; Hernández-Rodríguez, M.; Soler-Carracedo, K.; Lozano-Gorrín, A.; Lalla, E.; Chehimi, D. B. H. Synthesis, characterization and spectroscopic properties of a new Nd3 +-doped Co-picromerite-type Tutton salt. *J. Lumin.* **2016**, *177*, 93−98.
(17) Souamti, A.; Martín, I.; Zayani, L.; Lozano-Gorrín, A.; Chehimi, D. B. H. Luminescence properties of Pr3 + ion doped Mg-picromerite Tutton salt. *J. Lumin.* **2017**, *188*, 148−153.
(18) Abu El-Fadl, A.; Santos, I. C.; Paulo, A.; Nashaat, A. Enhanced physical properties of potassium zinc sulphate hydrate single crystal following iodide doping. *Mater. Res. Express* **2018**, *5*, No. 066207.
(19) Neto, J. G. O.; Viana, J. R.; Lopes, J. B. O.; Lima, A. D. S. G.; Sousa, M. L.; Lage, M. R.; Stoyanov, S. R.; Lang, R.; Santos, A. O. Crystal growth, crystal structure determination, and computational studies of a new mixed (NH4)2Mn1−xZnx(SO4)2(H2O)6 Tutton salt. *J. Mol. Model.* **2022**, *28*, No. 341.
(20) Souamti, A.; Zayani, L.; Palomino, J. M.; Cruz-Yusta, M.; Vicente, C. P.; Hassen-Chehimi, D. B. Synthesis, characterization and thermal analysis of K 2 M (SO 4) 2· 6H 2 O (M = Mg, Co, Cu). *J. Therm. Anal. Calorim.* **2015**, *122*, 929−936.
(21) Singh, B.; Gupta, S. P.; Khanna, B. N. The infrared spectra of tutton salts 1. A comparative study of (NH4)2 M″(SO4)2·6H2O (M″ = Ni, Co or Mg). *Pramana* **1980**, *14*, 509−521.
(22) Jayakumar, V. S.; Sekar, G.; Rajagopal, P.; Aruldhas, G. IR and polarized Raman spectra of (NH4) 2Mg (SO4) 2· 6 H2O. *Phys. Status Solidi A* **1988**, *109*, 635−640.
(23) Zhuang, X.; Su, G.; He, Y.; Zheng, G. Growth and characterisation of potassium cobalt nickel sulfate hexahydrate for UV light filters. *Cryst. Res. Technol.* **2006**, *41*, 1031−1035.
(24) Shen, Z.; Sherman, W. Structural transformation studies of AgNO3 by Raman and infrared spectroscopy. *J. Mol. Struct.* **1992**, *271*, 175−181.
(25) Huang, C.-H.; Brooker, M. Raman and ir spectroscopic studies of AgNO3 as the solid crystal and molten salt. *Spectrochim. Acta, Part A* **1976**, *32*, 1715−1724.
(26) Zaki, K.; Pouchan, C. Vibrational analysis of orthoboric acid H3BO3 from ab initio second-order perturbation calculations. *Chem. Phys. Lett.* **1995**, *236*, 184−188.
(27) Servoss, R. R.; Clark, H. Vibrational spectra of normal and isotopically labeled boric acid. *J. Chem. Phys.* **1957**, *26*, 1175−1178.
(28) Krishnan, K. The Raman spectrum of boric acid. *Proc. Indian Acad. Sci., Sect. A* **1963**, *57*, 103−108.
(29) Theo Kloprogge, J.; Ruan, H.; Frost, R. L. Near-infrared spectroscopic study of basic aluminum sulfate and nitrate. *J. Mater. Sci.* **2001**, *36*, 603−607.
(30) Bukas, V. J.; Tsampodimou, M.; Gionis, V.; Chryssikos, G. D. Synchronous ATR infrared and NIR-spectroscopy investigation of sepiolite upon drying. *Vib. Spectrosc.* **2013**, *68*, 51−60.
(31) Nakamoto, K. Infrared and Raman Spectra of Inorganic and Coordination Compounds. *Handbook of Vibrational Spectroscopy*; John Wiley & Sons, Inc., 2006.
(32) Minigalieva, I.; Katsnelson, B.; Privalova, L.; Sutunkova, M.; Gurvich, V.; Shur, V.; Shishkina, E.; Valamina, I.; Makeyev, O.; Panov, V.; et al. Attenuation of combined nickel (II) oxide and manganese (II, III) oxide nanoparticles' adverse effects with a complex of bioprotectors. *Int. J. Mol. Sci.* **2015**, *16*, 22555−22583.
(33) Xie, Y.; Guo, Y.; Guo, Y.; Wang, L.; Zhan, W.; Wang, Y.; Gong, X.; Lu, G. A highly effective Ni-modified MnO x catalyst for total oxidation of propane: the promotional role of nickel oxide. *RSC Adv.* **2016**, *6*, 50228−50237.
(34) Saravanan, K.; Jarry, A.; Kostecki, R.; Chen, G. A study of room-temperature LixMn1.5Ni0.5O4 solid solutions. *Sci. Rep.* **2015**, *5*, No. 8027.
(35) Martina, I.; Wiesinger, R.; Jembrih-Simbürger, D.; Schreiner, M. Micro-Raman characterisation of silver corrosion products: instrumental set up and reference database. *e-Preserv. Sci.* **2012**, *9*, 1−8.

https://doi.org/10.1021/acsomega.3c00622
ACS Omega 2023, 8, 17800−17808